Journal of Magnetics 1(2), 69-74 (1996)

Inter-Grain Exchange Interaction and Hysteresis Loops of Melt-Spun $Nd_{13}Fe_{77}B_{10}$

J. H. Min,*,* Y. B. Kim,* W. S. Park,** M. J. Park,** and Li Tian*****

* *Korea Research Institute of Standards and Science, Taejon 305-606, Korea*

** *Korea University, Seoul, Korea*

*** *Department of Physics, Jilin University, Changchun, 130023, P. R. China*

(Received 2 December 1996)

Hysteresis loops of melt-spun $Nd_{13}Fe_{77}B_{10}$ cooled down at remanent state were measured at 4.2 K and 250 K. The hysteresis loops were analysed on the basis of the Stoner-Wohlfarth (S-W) model, the inter-grain exchange coupled single domain (SD) model and micromagnetism. The coercivity higher than that predicted from the S-W model and the striking shift of the thin minor loop along the H-axis observed at the fields of $H_{max} = 4$ MA/m at 4.2 K indicated new evidences for the inter-grain exchange interaction. The S-W model failed in explaining the high $_iH_c$ and the shift of the thin minor loop. The exchange coupled SD model was found to explain the experimental results qualitatively without difficulties associated with the S-W model. The micromagnetic calculations using a finite element technique simulated the experimental results fairly well quntitatively.

1. Introduction

It is well established that the melt-spun Nd-Fe-B alloys are isotropic, and the high coercivity and the high energy product are related with extremely fine grain structure of the $Nd_2Fe_{14}B$ phase [1]. The grains contact each other (nearly stoichiometric alloy) [2] or are surrounded by a very thin Nd rich phase (hyper -stoichiometric alloys) [3]. It is believed in general that the domain wall pinning at the grain boundaries is the origin of high coercivity [3-4]. For hyper-stoichiometric alloys, J_r is about half of J_s as is predicted from the Stoner-Wohlfarth (S-W) model. For near-stoichiometric alloys, J_r increases beyond $J_s/2$ and $_iH_c$ decreases with decrease of the scale of the nanostructure below ~50 nm at room temperature [8], which is ascribed to the inter-grain exchange interaction [2]. The $Nd_2Fe_{14}B$ has an easy axis along the c-axis above 132 K and four easy axes tilted from the c-axis towards the ⟨110⟩ axes below the temperature [10].

This work presents new evidences for the inter-grain exchange interaction. The evidences include high coercivity higher than that the S-W model predicts and a striking shift of a thin minor loop along the H-axis at 4.2 K after cooling down at remanent state. Validity of the S-W model, the inter-grain exchange coupled single domain (SD) molel and micromagnetism for explaining the hysteresis loops was examined.

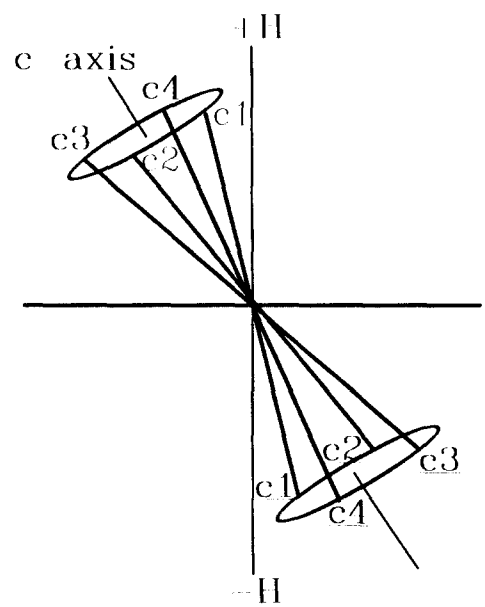

Fig. 1. Distribution of easy magnetization directions for $Nd_2Fe_{14}B$ below 132 K

2. Experiments

An amorphous alloy of nominal composition $Nd_{13}Fe_{77}B_{10}$ was prepared by a single wheel technique under argon atmos-

phere. The surface velocity of Cu wheel was 35 m/s and the alloy was 1 mm wide and ~30 μm thick. The alloy was annealed at 950 K (specimen #1) or 970 K (specimen #2) for 10 minutes in a vacuum of 1×10^{-4} Torr. The specimens were confirmed to be a $Nd_2Fe_{14}B$ single phase by X-ray diffaction. The strips were arranged into 5 mm-long, 3 mm-wide, 30 m-thick rectangular shape specimens. They were cooled down to 4.2 K at remanent state after magnetization along the ribbon length direction in a pulsed field of ~7 MA/m at room temperature. The hysteresis loops were measured along the ribbon length direction by a high field VSM (Janis 4500/150A).

3. Model and Calculations

A. Model and calculations

The model magnet is composed of $n \times n \times n$ cubic $Nd_2Fe_{14}B$ grains. Both of the c- and [100]-axes of the grains are randomly oriented. Each grain is exchange coupled with the six adjacent grains and is divided into $m \times m \times m$ cubic SD elements of equal dimension, so the magnet is divided into $mn \times mn \times mn$ ($mn = m \times n$) SD elements. The periodic boundary conditions hold for the magnet. By neglecting the magnetic stray-field energy [9], the total Gibb's energy, G, is

$$G = \sum_i [F_K(i) + F_H(i) + \frac{1}{2} F_X(i)] (\frac{L}{m})^3, \quad (1)$$

$$F_K(i) = K_1 sin^2\theta(i) + K_2 sin^4\theta(i) + K_3 sin^4\theta(i) cos(4\phi_i), \quad (2)$$

$$F_H(i) = -J_s(i) \cdot H, \quad (3)$$

$$F_X(i) = -\frac{w}{\mu_0} \frac{m}{L} \sum_{\text{adjac}} J_s(i) \cdot J_s(\text{adjacent element}), \quad (4)$$

where $F_K(i)$, $F_H(i)$, and $F_X(i)$ are the magnetocrystalline anisotropy energy, Zeeman energy and the exchange energy for the "i"th element, respectively, L is the dimension of a grain, $\theta(i)$ and $\phi(i)$ are the polar angles of the magnetization of the "i"th element in the $\langle 100 \rangle$ coordinate system, and w/μ_0 is the effective exchange constant per unit boundary area. The inter-element exchange interaction in a grain is assumed to be the same with that of inter grain exchange interacion. The values of J_s, K_1, K_2 and K_3 were taken from refs. [5-6] and are listed in Table 1. The value of w/L was estimated by fitting the calculated coercivity with the experimental value at 4.2 K.

The magnetization of the magnet, J, can be obtained from minimization of G. The energy of each element $G(i)$ should also be minimum to satisfy the above condition, i. e.

$$\delta G(i) = \delta[F_K(i) + F_H(i) + F_X(i)] = 0. \quad (i = 1, 2, \cdots, mn \times mn \times mn) \quad (5)$$

Table. 1. The values of J_s, K_1, K_2 and K_3 of $Nd_2Fe_{14}B$

temperature (K)	J_s[5] (T)	K_1	K_2	K_3 [6]
		(x 10^6 J/m^3)		
4.2	1.86	−16	27	0.45
250	1.57	6	1	0

Since there are many energy minimum states for a given H, care should be taken to assign correct initial magnetization distribution for each H and vary them along the track of the gradient of G to a new minimum energy state. Initially the magnet is saturated, then H is changed stepwise from H_{max} to $-H_{max}$ and then to H_{max}.

The S-W model is the case for $m = 1$ and $w = 0$, the exchange coupled SD model is the case for $m = 1$ and $w \neq 0$, and micromagnetic treatment is the case for $m > 1$ and $w \neq 0$.

B. Algorithm

Two methods were used. The first method is as follows. Let $\{\theta_0(i), \phi_0(i)\}$ ($i = 1, 2, \cdots, mn \times mn \times mn$) corresponds to an equilibrium state of the magnet for a given H. After H is changed, the first intermediate state $\{\theta_1(i), \phi_1(i)\}$ corresponding to the minimum of G within the variable range of $\{\theta_0(i) + \Delta\theta(i), \phi_0(i) + \Delta\phi(i)\}$ ($\Delta\theta(i), \Delta\phi(i) = 0, \pm 1$ degrees; $i = 1, 2, \cdots, mn \times mn \times mn$) is chosen. The same computation is repeated for the new state of $\{\theta_1(i), \phi_1(i)\}$ within the variable range of $\{\theta_0(i) + \Delta\theta(i), \phi_0(i) + \Delta\phi(i)\}$, and the second intermediate state $\{\theta_2(i), \phi_2(i)\}$ is obtained. Such process is repeated until G decreases to the final minimum and no further change of $\{\theta_1(i), \phi_1(i)\}$ occurs. This method needs to compute $(3 \times 3)^{mn \times mn \times mn}$ times for a cycle, which increases tremendously with increase of mn and consumes very large CPU time even for the simplest case of $mn = 2$. The method was used only for examination of the degree of approximation of the second method, which was used for real time computation in this work, for the simplest case of $n = 2$, $m = 1$ and $w \neq 0$.

For the second method, the first intermediate state of "i"th element, $\theta_1(i)$ and $\phi_1(i)$, is obtained from minimization of $G(i)$ within $\Delta\theta(i), \Delta\phi(i) = 0, \pm 1$ degrees under fixed magnetization of the other elements. For the new state of the "i"th element, the new state is chosen for an adjacent element. After a cycle of such computations through the $mn \times mn \times mn$ elements, G and normalized magnetization of the magnet, J/J_s, is calculated. The cycle of the computation is repeated until G decreases to a limit and stabilizes around it. For a cycle it needs $3 \times 3 \times mn \times mn \times mn$ times computations which is much smaller than that of the first method. This method does not take into account the possible concurrent variation of magnetization directions of some exchange coupled adjacent elements. As a result, G and J/J_s in general do not reach their stabilized values but fluctuate around their limit by a small amplitutes. The limit of G is larger than that obtained by the

first method. Figure 2 demonstrates the variation of G and J/J_s with the number of cycle. Table 2 demonstrates the specialization of the magnet for $n = 3$.

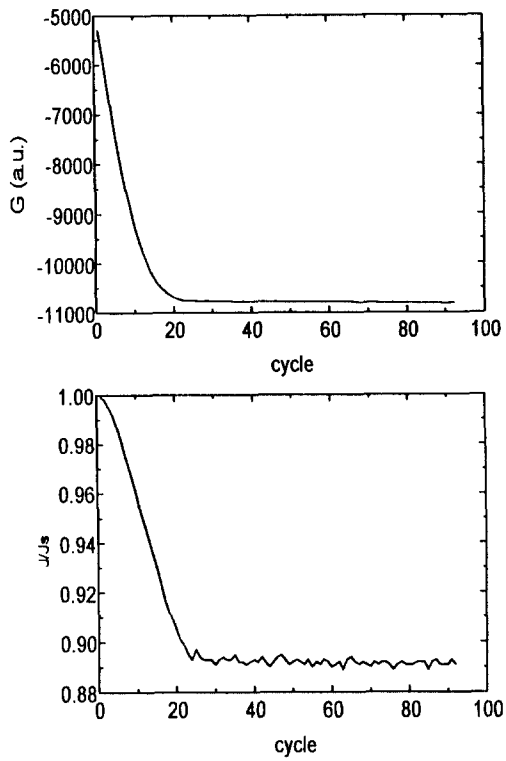

Fig. 2. G (a) and J/J_s (b) as a function of the number of cycle of computation

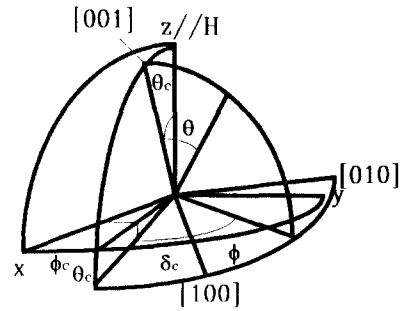

Fig. 3. Geometrical meaning of θ_c, ϕ_c, δ_c, θ, and ϕ

The geometrical meaning of the angles θ_c, δ_c and ϕ_c in the table along with θ and ϕ are presented in Figue 3.

Table 3 compares the stabilized states computed by the two methods for $n = 2$, $m = 1$ and $w = 1 \times 10^{-5}$ at $H = -0.87$ MA/m and 4.2 K. The state obtained for the second method corresponds to a minimum of G. It can be seen that all of θ and ϕ for grains 212, 221 and 222 obtained by the rigorous first method are larger than those obtained by the second method by one degree which state is never reached by using the second method.

4. Results and Discussions

A. Experimental results

Figures 4(a) shows the hysteresis loop measured at the fields of $H_{max} = 6.4$ MA at 4.2 K for specimen #2. The loop is not

Table Ⅱ. θ_c, ϕ_c and δ_c of the grains (i, j, k) (i, j, k = 1, 2, 3) for the magnet of $n = 3$

deg.	111	112	113	121	122	123	131	132	133	211	212	213	221	222	223	231	232	233	311	312	313	321	322	323	331	332	333
θ_c	60	90	60	90	30	60	90	60	30	60	0	60	90	60	90	30	60	30	90	60	30	60	30	60	90	30	60
ϕ_c	0	180	330	103	113	180	51	270	267	120	25	60	154	150	26	216	240	61	77	210	319	300	10	30	129	164	90
δ_c	41	8	16	45	15	30	8	4	38	25	0	0	0	41	38	23	29	30	15	20	21	33	8	12	23	0	37

Table Ⅲ. Comparison of the stabilized states computed by the two methods (θ and ϕ are in deg.)

method	G (a. u)	J/J_s	111		112		121		122		211		212		221		222	
			θ	ϕ	θ	ϕ	θ	ϕ	θ	ϕ	θ	ϕ	θ	ϕ	θ	ϕ	θ	ϕ
1	−454.1	.403	147	228	34	257	35	246	34	61	32	256	36	130	36	41	148	247
2	−453.0	.406	147	228	34	257	35	246	34	61	32	255	35	129	35	40	147	246

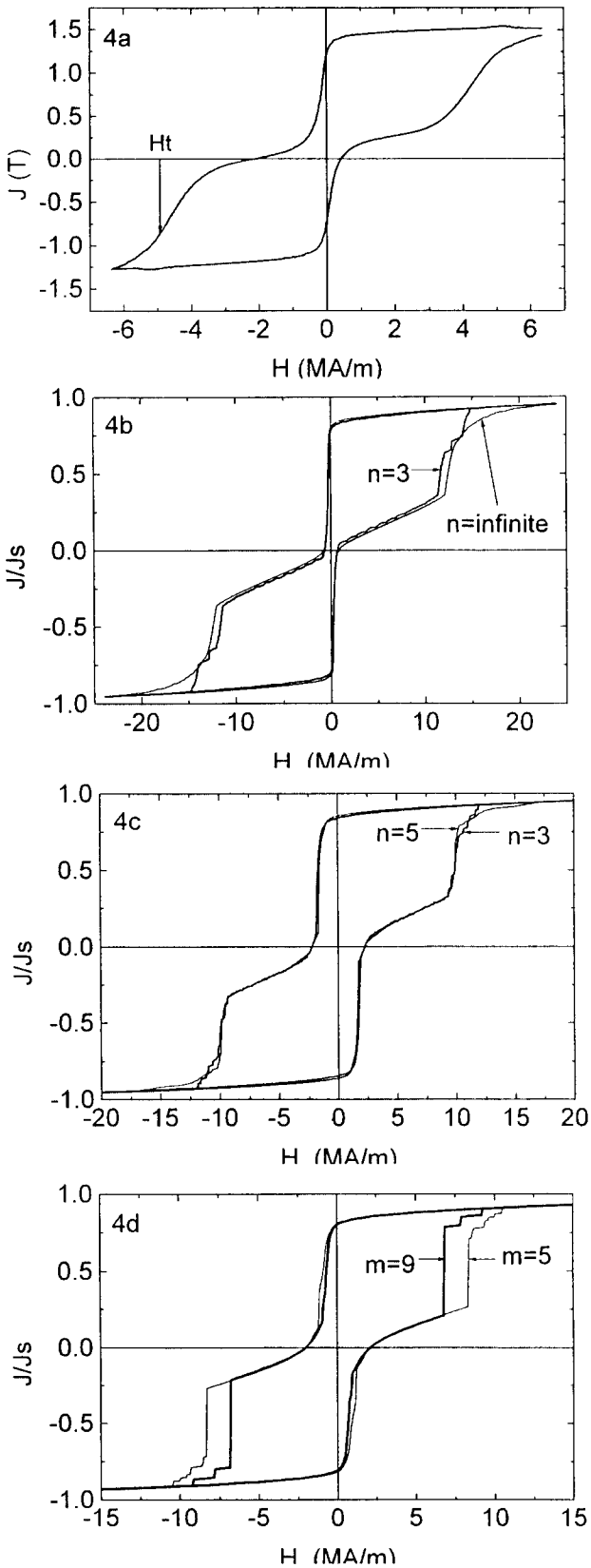

Fig. 4. Hysteresis loops at 4.2 K measured at the fields of H_{max} = 6.4 MA/m (a) and major hysteresis loops computed by the S-W model for $n = 3$ and ∞ (b), by the exchange coupled SD model for $n = 3$ ($w/L = 0.45$) and 5 ($w/L = 0.39$) (c), and by micromagnetism for $n = 3$ and $m = 5$ ($w/L = 0.32$) and $m = 9$ ($w/L = 0.29$) (d), respectively

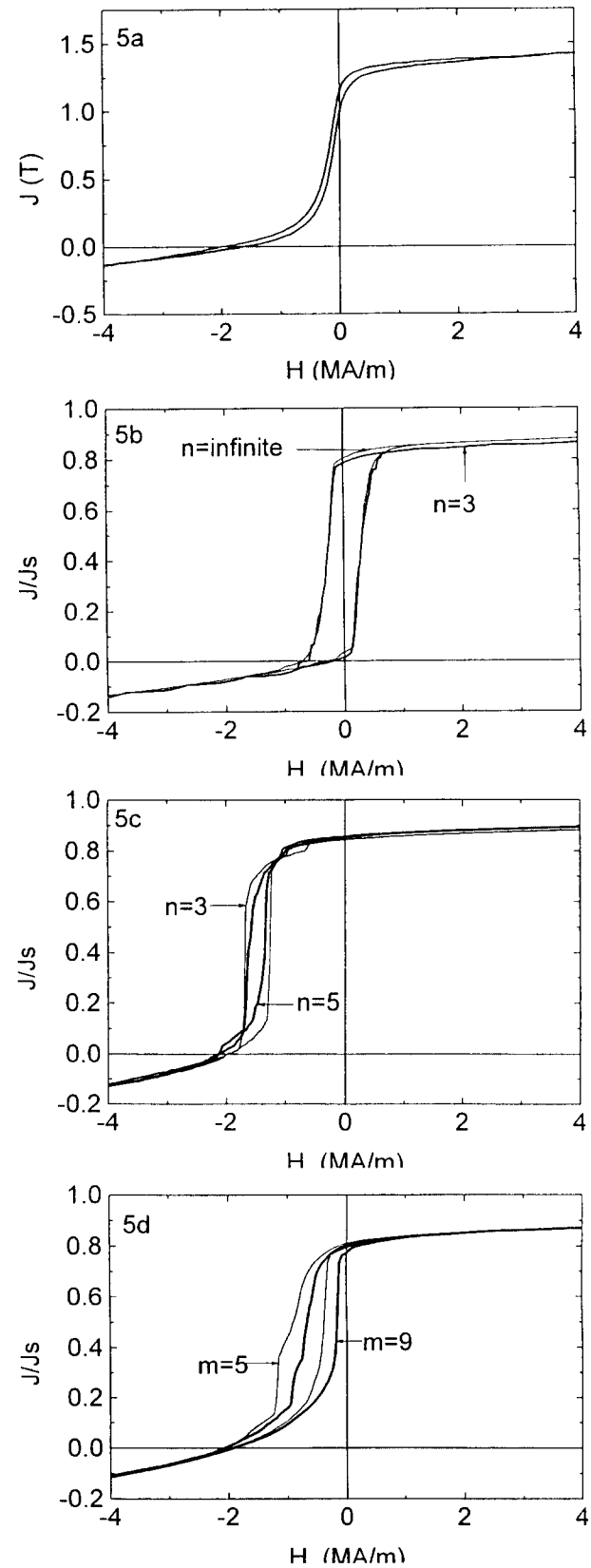

Fig. 5. Hysteresis loops at 4.2 K at the fields of H_{max} = 4.0 MA/m measured (a) and computed by the S-W model for $n = 3$ and ∞ (b), by the exchange coupled SD model for $n = 3$ ($w/L = 0.45$) and $n = 5$ ($w/L = 0.39$) (c), and by micromagnetism for $n = 3$ and $m = 5$ ($w/L = 0.32$) and $m = 9$ ($w/L = 0.29$) (d), respectively

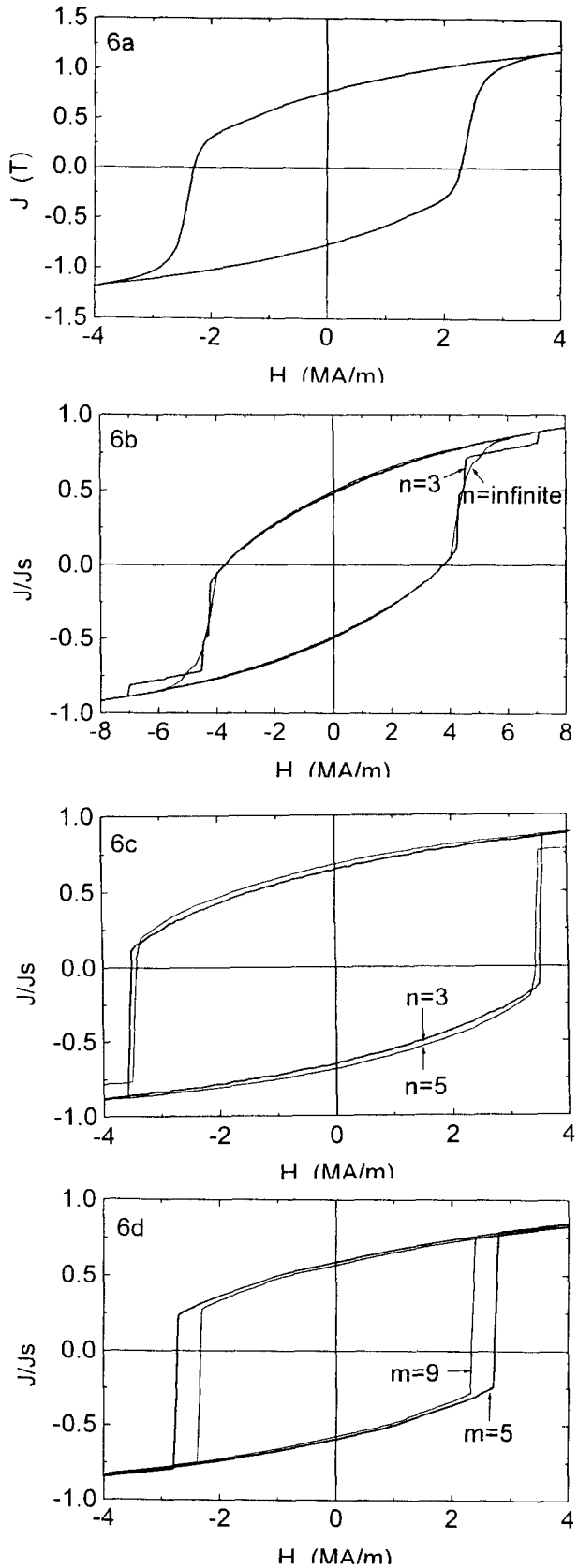

Fig. 6. Hysteresis loops at 250 K measured at the fields of $H_{max} = 4.0$ MA/m (a) and computed major hysteresis loops by the S-W model for $n = 3$ and ∞ (b), by the exchanged coupled SD model for $n = 3$ $(w/L = 0.45)$ and $n = 5$ $(w/L = 0.39)$ (c), and by micromagnetism for $m = 5$ $(w/L = 0.32)$ and $m = 9$ $(w/L = 0.29)$ (d), respectively

saturated and is asymmetrical. The two-step characteristic is observed, and this was reported by previous authors [7]. $_i H_c$ and the field corresponding to the middle of the high field step, H_t, are 2.2 MA/m and 4.8 MA/m, respectively. For specimen #1, $_i H_c = 2.0$ MA/m is smaller but $H_t = 5.3$ MA/m is larger than those for specimen #2.

Figure 5(a) is the minor loop for specimen #1 measured at the fields of $H_{max} = 4.0$ MA/m at 4.2 K. The hysteresis loop is very thin and shifted along both the J-axis and H-axis profoundly.

Figure 6(a) is the hysteresis loop for specimen #1 measured at the fields of $H_{max} = 4.0$ MA/m at 250 K. The hysteresis loop is characterized by the squareness which is typical for a permanent magnet.

B. Analysis by the S-W model

Figures 4(b), 5(b) and 6(b) show the computed major loops at 4.2 K, minor loops at 4.2 K and major loops at 250 K, respectively, for $n = 3$ and $n = \infty$. It is notable that the loops for such a small value of $n = 3$ are nearly the same with those for $n = \infty$.

Figure 4(b) reproduces the two-step characteristics of Figure 4(a) well. The computation shows that the low field step of the demagnetization curve is due to the two-step irreversible rotation of magnetization around the easy cone from the nearest to $+H$ easy direction $c1$ to $c2$ and then to $c3$, and the high field step represents irreversible rotation from $c3$ to the nearest to $-H$ easy direction $\underline{c1}$, oppositely directed counterpart of $c1$ (Figure 1). It is notable that the calculated value of $_i H_c = 0.6$ MA/m is unexpectedly much smaller than the experimental values of 2.0-2.2 MA/m. The value of $H_t \approx 13$ MA/m is two times larger than the experimental value.

Figure 5(b) is the minor loop at 4.2 K. It reproduces the upward shift of the thin minor loop at 4.2 K along the J-axis, but fails to reproduce the shift along the H-axis.

Figure 6(b) succeeds in simulating the square hysteresis loop. But the irreversible process occurs at the fields below $-_i H_c$ but not around $-_i H_c$ as is observed in Figure 6a. $_i H_c = 3.7$ MA/m is much larger than 2.3 MA/m of experiment.

C. Analysis by the exchange coupled SD modal

Figures 4(c), 5(c) and 6(c) show the computed major loops at 4.2 K, minor loops at 4.2 K and major loops at 250 K, respectively, for $n = 3$ and $n = 5$.

The major loop for $n = 3$ is essentially the same with that for $n = 5$. By taking into account the inter-grain exchange interaction, the value of $_i H_c$ could be increased to fit the experimental value of 2.0~2.2 MA/m by using the values of $\frac{w}{L} = 0.45$ for $n = 3$ and $\frac{w}{L} = 0.39$ for $n = 5$. With $L \approx 30$ nm [1-2], the exchange energy per unit area is ≈ 0.04 J/m^2.

The value is in accordance with $js^2/a^2 \approx 0.05$ J/m^2 estimated from the experimentally observed domain wall width $\delta \approx 3$ nm [3] by using the relation $\delta = \pi(Js^2/2aK_1)^{1/2}$ and the

values of $K_1 = 5 \times 10^6$ J/m^3 [6] and $a \approx 0.2$ nm. Here, Js^2 is the exchange energy for a pair and a is the distance between the pair.

After H is decreased from H_{max} to a low negative field where the demagnetization curve is in the second quarter, the inter grain exchange fields acting on most of the grains are positive, which prevent the low field irreversible magnetization rotation causing increase of $_iH_c$. On the other hand, in the third quarter the most of exchange fields are negative which causes decrease of H_t. Larger the value of the exchange interaction, larger the value of $_iH_c$ and smaller the value of H_t. The larger value of $_iH_c$ and smaller value of H_t for specimen #1 compared to those for specimen #2 reveals that the value of w/L for specimen #1 is larger than that for specimen #2.

Figure 5(c) shows that the shifted thin minor loop at 4.2 K (Figure 5a) can be explained by taking into account the inter grain exchange interaction. The width of the minor loop for $n = 5$ is smaller than that for $n = 3$. The shifted thin loop would be explained as follows. After H is decreased from H_{max} to −4.0 MA/m, a number of grains still remain positively magnetized. After H is increased, the positive exchange field acted by these grains promote their adjacent grains of irreversibly rotated magnetization to rotate back to positive field direction. Some adjacent grains rotate back in this way, which then causes some their adjacent grains to rotate back. Many grains rotate back in success in this way causing narrowing of the minor loop and so the shift of the minor loop.

Figure 6(c) shows that the exchange coupled SD model improves the simulation of the loop at 250 K in two ways. One is the occurrence of the irreversible process around $-_iH_c$ but not below $-_iH_c$. Another is decrease of the value of $_iH_c$.

D. Analysis by micromagnetism

Figures 4(d), 5(d) and 6(d) show the computed major loops at 4.2 K, minor loops at 4.2 K and major loops at 250 K, respectively, for for $n = 3$ and $m = 5$ and $m = 9$. The fitted values of w/L are 0.32 and 0.29 for $m = 5$ and 9, respectively. The quantitative simulation of the experiments is improved significantly.

H_t is decreased to 7.4 MA/m for $m = 5$ and further to 6.7 MA/m for $m = 9$. But they are still larger than ~5 MA/m of experiment. The calculated H_t approaches to the experimental value when m increases to about 13. The calculation, however, is very time consuming. and the work is under way.

The low field step begins near $H = 0$ and the slope of the steep part of the loop decreases in accordance with the experiment. Larger the value of m, better the simulation.

$_iH_c$ at 250 K are decreased to 2.7 MA/m and 2.3 MA/m for $m = 5$ and 9, respectively. The latter agrees with experiment well.

In summary, The S-W model can explain the main characteristics of the hysteresis loops qualitatively except the large coercivity and the shift of the thin minor loop along the H -axis at 4.2 K.

It has been accepted and confirmed by experiment that the S-W model presents the theoretical upper limit of $_iH_c$ for the case of uniaxial anisotropy. Contrary, this work suggests that the S-W model presents theoretical lower limit for the case of cone anisotropy.

The difficulties met by the S-W model in explaining the experiments are caused by neglection of the inter-grain exchange interaction and the exchange coupled SD model overcomes the difficulties. The model also improves the simulation of the loops quantitatively.

The micromagnetic model with limited values of n and m simulates the hysteresis loops much better than the exchange coupled SD model does. The simulation improves with increase of n and m. The magnetization proceeds by non-uniform magnetization rotation.

Acknowledgement

This work was supported by Brain Pool Project of the Korean Federation of Science and Technology Society and the National Science Foundation of China.

References

[1] A. Manaf, R. A. Buckley, H. A. Davies and M. Leonowicz, J. Magn. Magn. Mater., **101**, 360 (1991).
[2] G. B. Clemente, J. E. Keem and J. P. Bradley, J. Appl. Phys., **64**, 5299 (1988).
[3] R. K. Mishra, J. Magn. Magn. Mater., **54-57**, 450 (1986).
[4] F. E. Pinkerton and C. D. Fuerst, J. Appl. Phys., **67**, 4753 (1990).
[5] S. Hirosawa, Y. Matsuura, H. Yamamoto, S. Fujumura and M. Yamauchi, J. Appl. Phys., **59**, 873 (1986).
[6] M. Sagawa, S. Hirosawa, H. Yamamoto, S. Fujimura, M. Sagawa and Y. Matsuura, Jpn. J. Appl. Phys., **6**, 785 (1987).
[7] F. E. Pinkerton, J. Appl. Phys., **64**, 5565 (1988).
[8] A. Manaf, R. A. Buckley,H. A. Davis and M. Leonowicz, J. Magn. Magn. Mat., **101**, 360 (1991).
[9] H. Fukunaga and H. Inoue, Jpn. J. Appl. Phys., **31**, 1347 (1992).
[10] J. M. Cadogan, J. P. Gavigan, D. Givord and H. S. Li, J. Phys. F:Mt. Phys. **18**, 779 (1988).